Brillouin scattering study of the elastic properties of incommensurate barium sodium niobate

G. Errandonea, M. Hebbache, and F. Bonnouvrier

Centre National d'Etudes des Telecommunications, 196 rue de Paris, 92220 Bagneux, France

(Received 12 November 1984; revised manuscript received 15 April 1985)

The elastic properties of incommensurate barium sodium niobate (BSN) are investigated with Brillouin scattering. The velocities, linewidths, and related elastic constants of the main acoustic modes propagating in the (001) plane are measured between 20 and 500 °C across the normal-incommensurate transition and the lock-in transition. The main anomalies are observed for the elastic constants C_{11} and C_{22}. They exhibit a complex temperature dependence dominated by a large thermal hysteresis of a specific type and a high sensitiveness to the experimental procedure. A memory effect similar to the one observed by optical birefringence is described. From a theoretical point of view, the elastic behavior of BSN is derived in the framework of the standard Landau theory. This theory does not provide a good description of the experimental data. Instead, one obtains a good quantitative agreement in the normal phase and semiquantitative agreement in the incommensurate phase by considering three types of corrections: a coupling between the strains and the fluctuations of the order-parameter modulus, a dispersive coupling between the strains and the amplitude mode, and the influence of the defects. In particular, we show that the elastic anomalies induced by the defects are correlated to the anomalies observed with optical birefringence.

I. INTRODUCTION

In the last few years several experimental and theoretical works have been devoted to the study of the elastic properties of insulating materials undergoing incommensurate transitions. According to the symmetry properties of the incommensurate order parameter (OP) and of the elastic strains, various types of acoustic anomalies can be observed at the normal-incommensurate transition (NIT) and at the lock-in transition (LIT). A review of this topic can be found in Refs. 1 and 2.

In this paper we report on a detailed Brillouin scattering study and a phenomenological interpretation of the acoustic properties of barium sodium niobate, $Ba_2NaNb_5O_{15}$ (BSN), on both sides of its NIT and LIT. It is interesting to consider this material since it possesses two important peculiarities with respect to other insulating incommensurate materials. On the one hand, it is the only confirmed example[3−5] displaying a point symmetry change at the NIT, while such a change only occurs at the LIT in other known systems. This characteristic is a consequence of an unusual, but not unique, circumstance: the four dimensionality of the OP related to the incommensurate phase (INCP). On the other hand, BSN shows a set of phenomena related to the presence of the INCP, but departing from the standard behavior expected for incommensurate systems. These phenomena,[6,7] which include a large thermal hysteresis of a specific type, slow time-relaxation processess, and a "memory effect," are currently assigned to the occurrence of an interaction between the incommensurate modulation and mobile point defects. Similar phenomena have been pointed out in other substances,[8−11] but in BSN their amplitude is larger by an order of magnitude.

BSN belongs to the family of mixed oxide compositions which crystallizes with the tetragonal tungsten-bronze structure.[12] An intricate pattern of structural transitions has been observed in it. A standard ferroelectric transition[13] ($P4/mbm \rightarrow P4bm$) occurs at about 580 °C. The NIT and the LIT are located[3,4] near 300 and 270 °C, respectively, and surround an INCP possessing an average orthorhombic $mm2$ point symmetry; however, the precise range of stability of this INCP varies widely with the conditions of the measurements.[6] The orthorhombic symmetry persists down to −160 °C, at which an other transformation restores a tetragonal symmetry.[14]

The main static and dynamic characteristics of the INCP have been determined using x-ray and neutron measurements.[3,4] The NIT is continuous and is induced by the condensation of a soft optic mode whose wave vector is

$$\mathbf{k}_i = (1+\delta) \left[\frac{\tilde{\mathbf{a}}^* + \tilde{\mathbf{b}}^*}{4} \right] + \frac{\mathbf{c}^*}{2}, \tag{1}$$

with $\delta \sim 0.125$, $\tilde{\mathbf{a}}^*$, $\tilde{\mathbf{b}}^*$, and $\tilde{\mathbf{c}}^*$ being the reciprocal-lattice vectors of the tetragonal normal crystalline phase (NP) stable above T_i. Structural data[12] suggest that the atomic displacements related to this displacive transition consist of a collective shearing of the oxygen octahedra which form the skeleton of the BSN structure.

In the INCP the wave vector of the incommensurate modulation is also given by (1). On heating, δ linearly increases from 0.08 at T_L to 0.125 at T_i. Unlike the situation in most other substances, the lock-in of the modulation on a simple surstructure at T_L is incomplete; the phase stable below T_L possesses a small residual incommensurability ($\delta \sim 0.01$). It will be designated hereafter as the quasicommensurate phase of BSN (QCP).

The onset of the incommensurate modulation, directed

along one bisector of the tetragonal $\tilde{a}$ and $\tilde{b}$ axes, breaks the macroscopic equivalence between the two bisectors and sets in the system an "average" $mm\,2$ point symmetry in which the orthorhombic axes $(\mathbf{a},\mathbf{b})$ are turned by 45° with respect to the tetragonal ones of the NP. Hence, the NIT is also a ferroelastic transition. Accordingly, ferroelastic domains[15] and macroscopic quantities such as the birefringence[6] $n_a - n_b$, the shear strain[16] $e_1 - e_2$, and the elastic anisotropy[17-19] ($C_{22} - C_{11}$) spontaneously occur at T_i.

Several studies[17-20] of the elastic properties of BSN near 300 °C have been performed between 1970 and 1976, before the discovery of the INCP. More recently, Young and Scott[21] have measured the wave-vector dependence of the longitudinal-acoustic modes propagating along the orthorhombic a and b directions. They found a dispersion of the elastic constants c_{11} and c_{22} in the range 5—65 GHz on both sides of the NIT. In the INCP, they assigned its origin to a coupling of the acoustic modes with the amplitude mode and the phase mode, but they did not explain the dispersion in the NP.

In this paper we reexamine in a more complete way the elastic properties of BSN with an improved accuracy and with special care regarding the thermal history of the investigated samples. Unusual effects related to the interaction between the modulation and mobile defects are shown. The experimental procedure is described in Sec. II and our results are presented in Sec. III. In Sec. IV we present a phenomenological Landau theory of the elastic constants of BSN. The predictions of this standard theory only account for the broad features of the experimental data relative to several elastic constants and do not provide a detailed description of their behavior. Therefore to obtain a better agreement, in a second step, we describe in Secs. V and VI the influence of three types of effects: the fluctuations of the OP at the NIT, the dispersive coupling[21] between the OP and the overdamped amplitude mode,[3,22] and the role of the defects.[6]

II. EXPERIMENTAL PROCEDURE

A. Instrumental setup

The main features of a Brillouin scattering experiment have often been described.[23] Our setup is schematically represented in Fig. 1. The excitation was provided by a 300-mW, linearly polarized, single-mode line of a CR8 argon laser emitting at 5145 Å, focused on the sample with a beam diameter of ~ 60 μm. To improve the consistency of different measurements, acoustic modes propagating along perpendicular directions were sometimes simultaneously observed using a 10-cm-focal-length spherical mirror which reflected the beam emerging from the sample (Fig. 4). Thus, the sample could be excited by two collinear beams propagating in opposite directions.[18]

The light scattered at a right angle by a volume of size $\sim 60 \times 60 \times 150$ μm^3 was collected with a 17-mrad acceptance and analyzed by means of a three-pass, pressure-scanned, Fabry-Perot interferometer (free spectral range: 75 Ghz; finesse: 95; contrast: 10^6). In BSN one has intense Raman scattering lines which cannot be sufficiently
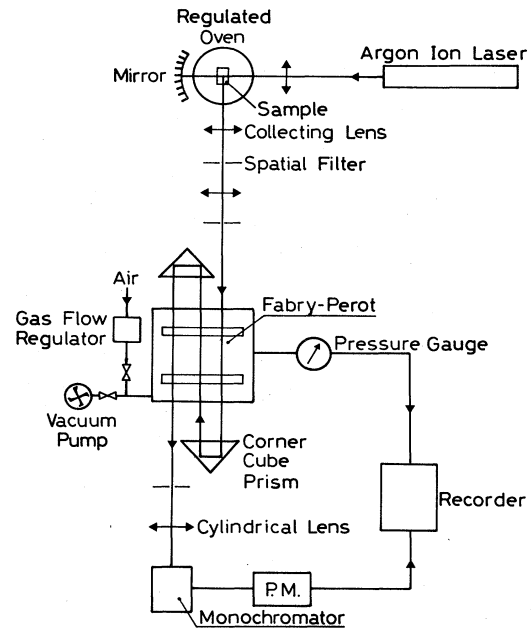

FIG. 1. Experimental setup. The spectral analysis is performed with a three-pass, pressure-scanned Fabry-Perot interferometer. Brillouin shifts are deduced from the measurements of the pressure in the Fabry-Perot tight cell.

suppressed by a mere interference filter. For this reason, we have used as a filter a Jarrell-Ash grating monochromator with a bandwidth of ± 10 cm^{-1}. The analyzed light was then detected with a R649 Hamamatsu photomultiplier (S20 photocathode) cooled to -60 °C by a gaseous nitrogen flow, followed by a 9511 Brookdeal photoncounter. The background signal was about 5 photons/sec and the fluctuation signal-to-noise ratio was reduced to 2% using a 1-sec time-constant integrator.

Brillouin spectra were linearly frequency-scanned with a 4-Ghz/min rate using a gas-flow regulator. Brillouin-shift frequencies were deduced from the measurement of the pressure in the Fabry-Perot tight cell performed with a Sensotec pressure transducer with an accuracy of ± 0.5 mbar corresponding to ± 80 MHz.

We used three parallelepipedic samples of approximate size $3 \times 3 \times 5$ mm^3, grown by the Czochralski method. The two first samples were cut from commercially purchased boules grown by the CGE Company (France) and the third one was grown in our laboratory. Like all real samples of BSN, their chemical compositions depart from the stoichiometric formula $Ba_2NaNb_5O_{15}$. The composition, the density at room temperature, and the orientations of the three investigated samples are listed in Table I.

The two chosen orientations permitted measurement of the sound velocities of the Brillouin-active modes propagating along the [100], [010], and [110] directions (referred to the orthorhombic axes). The scattering geometries are indicated in Table II, where we label the acoustic modes with the γ_i notation previously defined by Vacher and Boyer.[24] The transverse modes γ_2, γ_6 (in both phases), and γ_{11} (only in the quadratic phase) are inactive in the investigated geometries.

TABLE I. Characteristics of the investigated samples. Chemical compositions have been measured using a Castaing microsonde. Directions are referred to the orthorhombic axes.

Samples	Composition	Room-temperature density	Face orientation
1	$Ba_{2.07}Na_{0.88}Nb_{5.00}O_{15}$	5.30 ± 0.03	$[110], [1\bar{1}0], [001]$
2	$Ba_{2.10}Na_{0.87}Nb_{4.99}O_{15}$	5.30 ± 0.03	
3	$Ba_{2.06}Na_{0.83}Nb_{4.99}O_{15}$	5.35 ± 0.01	$[100], [010], [001]$

The samples studied contained both ferroelectric and ferroelastic domains. The two types of ferroelectric domains[13] (which differ by the orientation of the ferroelectric polarization along [001] or [00$\bar{1}$]) possess the same elastic and photoelastic properties and cannot be distinguished by Brillouin scattering measurements. Similarly, the [110] and [1$\bar{1}$0] sound-propagation directions are equivalent for the two types of ferroelastic domains (whose respective orientations are perpendicular). By contrast, the [100] and [010] directions correspond to different Brillouin spectra which can be mixed when the scattering volume contains the two types of ferroelastic domains. Fortunately, we were generally able to find some areas in the samples containing a large proportion of only one type of ferroelastic domain, whatever the temperature (it had been noted previously[3] that the domain pattern is insignificantly altered in BSN after each incursion in the tetragonal phase on crossing the ferroelastic transition).

The instrumental linewidth (full width at the middle height) measured for the Rayleigh line was 800 MHz, but the nonzero value of the collection solid angle induced an additional cause of widening of the Brillouin lines. This widening was negligible for the transverse-acoustic mode of BSN. It increased the apparent instrumental linewidth in the spectral range of the longitudinal modes to 1.2 GHz.

Samples were heated in a silver furnace provided with four apertures in the directions of the exciting and analyzed beams. The temperature of the samples was regulated with a stability of $\pm 0.1\,°C$ $(\Delta T/T_c \approx \pm 1.5 \times 10^{-4})$ and measured with a 7-mm-long, 100-Ω platinum resistor in contact with the crystals. Sample heating by laser beam was found to be negligible since the measurements of some Brillouin-shift frequencies having a pronounced dependence on temperature were found to be reproducible on lowering the laser-beam power from 300 to 100 mW.

B. Velocity measurements

Birefringence and x-ray measurements[6,7] have shown that the physical properties of BSN are very dependent on the experimental procedure. In particular, the results were shown to depend on the heating or cooling rates of the sample's temperature. Besides, a strong hysteresis has been evidenced in the INCP. As a consequence, most of our measurements were performed with the following procedure: the trend of variations of the temperature was

never reversed between 20 and 350 °C; the temperature was kept constant during the time of the measurements (20 min) and varied with a rate of 2.5 °C/min between two measurements. Hence, we estimate the average rate of the temperature variations to be approximately 0.3 °C/min.

Sound velocities v were deduced from Brillouin shifts Δv using

$$v = c \frac{\Delta v}{v_L}(n_i^2 + n_d^2)^{-1/2} , \tag{2}$$

where v_L is the frequency of the incident light, c is the light velocity in vacuo, and n_i and n_d are, respectively, the refractive indices for the incident and scattered beams (the scattering angle is 90°). We used the values of the refractive indices measured by Singh[13] at 5145 Å: $n_x = 2.3786$, $n_y = 2.3767$, and $n_z = 2.2583$ at room temperature, and we took into account the relatively large temperature dependence of these indices $(\Delta n_z/n_z \approx 3\%$ between 20 and 500 °C) which is known for this material.[20]

C. Derivation of the elastic constants

From the measurements of the velocities of the observed acoustic modes, we can deduce the values of several elastic constant of BSN: C_{11}, C_{22}, C_{44}, C_{55} (referred to the orthorhombic frame of BSN), and $\tilde{C}_{11}$ (referred to the tetragonal frame, deduced from the orthorhombic one by a 45° rotation around the c axis), with the help of the eigenvalue equation:[25]

$$\det \left| \sum_{j,k=1}^{3} C_{ijkl}^* - \rho v^2 \delta_{il} \right| = 0 , \tag{3}$$

where ρ is the density of the sample, δ_{il} is the Kronecker symbol, and the C_{ijkl}^* are effective elastic constants.

We used the room-temperature values of the densities listed in Table I and estimated their temperature dependences with the help of the available dilatometric data of Abell.[26] The C_{ijkl}^* constants correspond to the electric neutrality $(\text{div } \mathbf{D} = 0)$ and to adiabatic conditions, while the phenomenological theories of phase transitions refer to the isothermal elastic constants at constant electric field, or at constant electric polarization. Piezoelectric and adiabatic-isothermal corrections have to be taken into account to derive the latter quantities from the experimental data.

The piezoelectric correction is given[25] by

TABLE II. Scattering geometries and expressions of ρv^2 as a function of the elastic constants for the observed acoustic modes, in a reference frame constituted by the **a,b,c** orthorhombic axes. In the first several columns, we indicate the number of the sample, the directions of the incident and scattered beams, and their respective polarizations. In the next three columns, we give the direction of the propagation, the polarization (L for longitudinal modes, T for transverse or quasitransverse modes) and the labeling (following the notation of Ref. 24) of the investigated acoustic modes. (Pol. denotes polarization.)

Samples	Scattering geometries				Observed acoustic modes			ρv^2	
	q_i	q_s	e_i	e_s	Q	Pol.	Mode	Orthorhombic phase	Quadratic phase
1,2	[110]	[$\bar{1}$10]	[001]	[001]	[100]	L	γ_i	C_{11}	C_{11}
				[110]		T	γ_3	$C_{55}+e_{15}^2/\epsilon_{11}$	$C_{44}+e_{24}^2/\epsilon_{11}$
1,2	[$\bar{1}$10]	[110]	[001]	[001]	[010]	L	γ_4	C_{22}	C_{11}
				[1$\bar{1}$0]		T	γ_5	$C_{44}+e_{24}^2/\epsilon_{22}$	$C_{44}+e_{24}^2/\epsilon_{11}$
3	[110]	[010]	[001]	[001]	[110]	L	γ_{10}	$\frac{1}{4}\{C_{11}+C_{22}+2C_{66} +[(C_{11}-C_{22})^2+4(C_{12}+C_{66})^2]^{1/2}\}$	$(C_{11}+C_{12})/2+C_{66}=\widetilde{C}_{11}$
				[001]		T	γ_{11}	$\frac{1}{4}\{C_{11}+C_{22}+2C_{66} -[(C_{11}-C_{22})^2+4(C_{12}+C_{66})^2]^{1/2}\}$	$(C_{11}-C_{12})/2+C_{66}$ (inactive)
				[100]		T	γ_{12}	$\frac{1}{2}[C_{44}+C_{55} +(e_{15}+e_{24})^2/(\epsilon_{11}+\epsilon_{22})]$	$C_{44}+e_{24}^2/\epsilon_{11}$

$$C_{ijkl}^{*} - C_{ijkl}^{E} = \frac{\sum\limits_{m,n=1}^{3} e_{m,ij} e_{n,kl} Q_m Q_n}{\sum\limits_{m,n=1}^{3} \epsilon_{mn} Q_m Q_n} , \tag{4}$$

where $e_{m,ij}$, ϵ_{mm}, and C_{ijkl}^{E} are the respective components of the piezoelectric-, dielectric-, and elastic-stiffness- (at constant electric field) constant tensors. Throughout this paper, we shall omit the superscript E for simplification, and we shall write C_{ijkl} instead of C_{ijkl}^{E}.

The expressions of ρv^2 for the observed acoustic modes in the orthorhombic and quadratic phases, deduced from the Eqs. (3) and (4), are given in Table II. The piezoelectric corrections only affect the elastic constants C_{44} and C_{55}. On the basis of the consistent piezoelectric and dielectric results of Warner[27] and of Yamada,[20] we found that e_{24}^2/ϵ_{22} decreases from 4×10^9 to 2×10^9 N/m² between 20 and 500 °C, while e_{15}^2/ϵ_{11} is always included between 2 and 2.5×10^9 N/m². These corrections contribute to 6—3 % of the values of C_{44} and C_{55}.

The adiabatic-isothermal correction is given[28] by the relation

$$\Delta C_{ij} = C_{ij}^{S} - C_{ij}^{T} = \frac{T}{C_s} \left[\sum_{k=1}^{3} C_{ik} \frac{de_k}{dT} \right] \left[\sum_{k'=1}^{3} C_{jk'} \frac{de_{k'}}{dT} \right] , \tag{5}$$

where C_s is the specific heat (at clamped strains) and the de_k/dT are the expansion coefficients. C_{44} and C_{55} are not affected by this correction. For C_{11}, C_{22}, and $\widetilde{C}_{11}$, this correction cannot be accurately calculated since, to our knowledge, the specific heat of BSN has never been measured. On the basis of the Einstein model[29] of the specific heat and of the known Raman spectra,[30] we estimate an order of magnitude of $C_s/T \approx 5 \times 10^3$ J m⁻² K⁻¹. We use the room-temperature values of C_{12}, C_{13}, and C_{23} measured by Warner[27] (see Table VII), and we neglect their unknown temperature dependences. We found that ΔC_{11}, ΔC_{22}, and $\Delta \widetilde{C}_{11}$ are, respectively, close to 4.4×10^9, 3.4×10^9, and 3.9×10^9 N/m² ($\sim 1.5\%$ of the values of C_{11}, C_{22}, and $\widetilde{C}_{11}$) between 20 and 220 °C. In the INCP these quantities vary more strongly with the temperature because of the pronounced temperature dependence of the expansion coefficients. They are always smaller than 8×10^9 N/m². However, the accuracy of Abell's data is not sufficient to deduce a good estimation of the corrections in this phase. In the quadratic phase the three adiabatic-isothermal corrections are equal and slowly decrease from 3.1×10^9 to 1.9×10^9 N/m² between 310 and 520 °C.

III. EXPERIMENTAL RESULTS

A. Acoustic-mode frequencies and linewidths

We have mainly focused our attention on the longitudinal γ_1 and γ_4 modes, related to the C_{11} and C_{22} elastic constants of BSN. In this section we shall successively present (1) the characteristics of these two modes measured during a typical heating-cooling cycle, (2) unusual effects showing the sensitivity of the results to the experi-
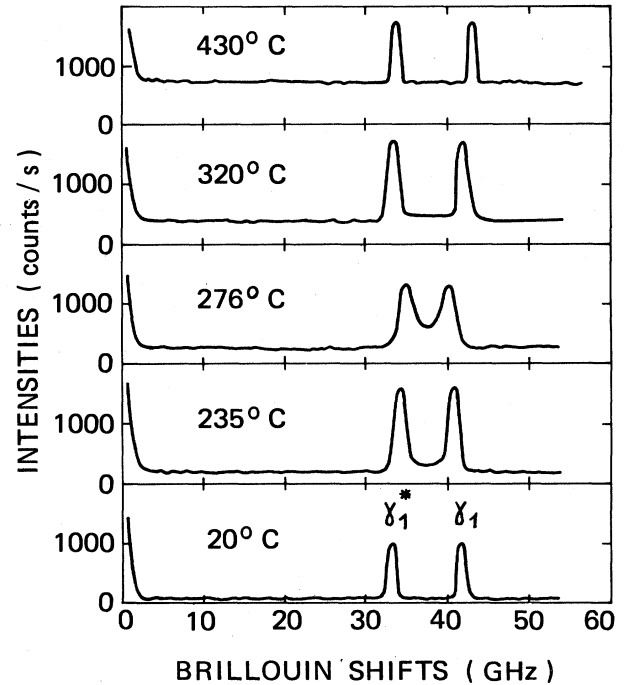

BRILLOUIN SHIFTS (GHz)

FIG. 2. Temperature dependence of the Brillouin spectra relative to the γ_1 mode in the $y -x (z,z)y +x$ scattering geometry. γ_1^* is the anti-Stokes line. One can note a minimum of the γ_1-mode frequency near 276 °C and an increase of the background intensity on heating.

mental conditions, and (3) the properties of the other investigated modes.

1. Characteristics of the γ_1 and γ_4 modes

First, we have measured the temperature dependence of the frequencies and the linewidths of these two modes on cycling thermally sample 1 between 20 and 480 °C at an average heating-cooling rate of nearly 0.3 °C/min as discussed in Sec. II B. Typical Brillouin spectra relative to the γ_1 mode are shown in Fig. 2.

The temperature dependences of the γ_1-mode and γ_4-mode frequencies are plotted in Fig. 3. On the heating run, these frequencies reach a minimum at 273 and 298 °C, respectively. On the cooling run, the temperatures at which the minima occur are shifted down to ~ 220 and 275 °C. The ferroelastic transition (NIT) temperature can
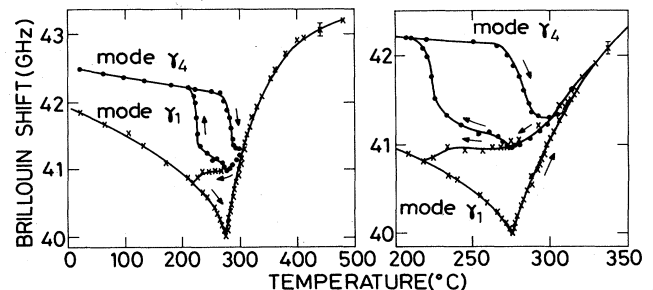

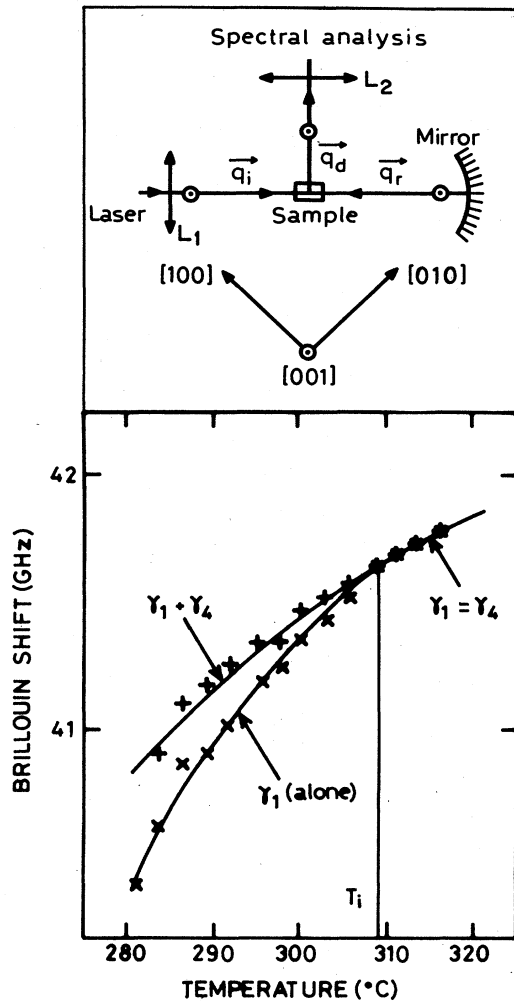FIG. 3. Temperature dependences of the frequencies of the γ_1 and γ_4 modes.

FIG. 4. Localization of the NIT temperature. Upper: the γ_1 and γ_4 modes are simultaneously observed with the help of a mirror located behind the sample. Lower: temperature dependences of the frequencies at which the intensities of the γ_1 line (alone) and of the γ_1 and γ_4 lines (observed together) are maximum. These frequencies merge at $T_i = (309\pm1)\,°C$.

be determined as the temperature where the frequencies of both modes become equal[18] ($C_{11} = C_{22}$). This temperature has been carefully measured using the backreflector mirror which permits accurate observation of the merging
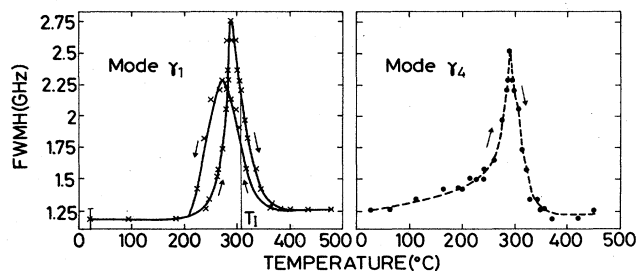

FIG. 5. Temperature dependences of the apparent linewidths of the γ_1 mode (crosses) and the γ_4 mode (dots). The instrumental linewidth is 1.2 GHz.

of the γ_1 and γ_4 lines (see Fig. 4). On heating, we locate the NIT at $309\pm1\,°C$. On cooling, a clear separation of the two lines occurs only near 275 °C. The localization of the LIT temperature cannot be determined on the sole basis of the present experimental data. Birefringence and x-ray measurements[6,7] performed with a comparable temperature-variation rate show that they are, in fact, located near 275 °C on heating and near 225 °C on cooling.

The behavior of the γ_1- and γ_4-mode frequencies is dominated by a large thermal hysteresis ($\sim 100\,°C$). It begins very unusually in the tetragonal phase near 325 °C, some 16 °C above the continuous NIT, and ends at about 215 °C.

The temperature dependences of the γ_1- and γ_4-mode widths are plotted in Fig. 5. Far from the incommensurate transitions ($T < 200\,°C$ or $T > 400\,°C$), the measured widths are equal to the instrumental linewidth (1.2 GHz). On heating up from room temperature, they increase to reach a maximum (~ 2.75 GHz) near 288 °C, inside the stability range of the incommensurate phase, some 20 °C below the NIT. On cooling, we could not perform accurate measurements of the γ_4-mode width since the examined scattering volumes always contained some domains of perpendicular orientation, leading to a contamination of the γ_4 line by the much stronger γ_1 line. The behavior of the γ_1-mode width is less sharp than on heating with a maximum at 2.3 GHz reached near 275 °C.

2. Influence of the experimental conditions

The temperatures and the amplitudes of the different anomalies discussed above are not reproducible in the sense that they are dependent on the experimental procedure. Such a sensitivity on the experimental conditions has already been observed in the measurements[6,7] of several physical quantities of BSN (spontaneous birefringence, dielectric constant, incommensurate satellites). It has been interpreted in terms of a strong interaction between the incommensurate modulation and mobile defects, inducing the slow diffusion of defects which form a defect density wave patterned after the modulation. As a consequence, birefringence and x-ray measurements have showed a large and unusual thermal hysteresis in BSN, a relaxation effect (consisting of a slow evolution with respect to time of some physical properties), and a memory effect. We have looked for such effects in the behavior of the γ_1 and γ_4 modes of sample 1.

A first unusual feature of the hysteresis was already noticed above: the hysteresis begins in the tetragonal phase above the continuous NIT. A second nonclassical property was evidenced on the measurements of the γ_4-mode frequency by reversing the variation trend of the temperature in the range of stability of the INCP (points A, B, and C in Fig. 6). For a usual hysteresis (related to a first-order transition), we expect that this procedure would lead to an exact coincidence of the measurements performed on the heating and cooling runs and, therefore, to an apparent suppression of the thermal hysteresis. By contrast, we obtain the intermediate dashed AA', BB', and CC' curves, which reveal the existence of a variety of metastable states in this temperature range.
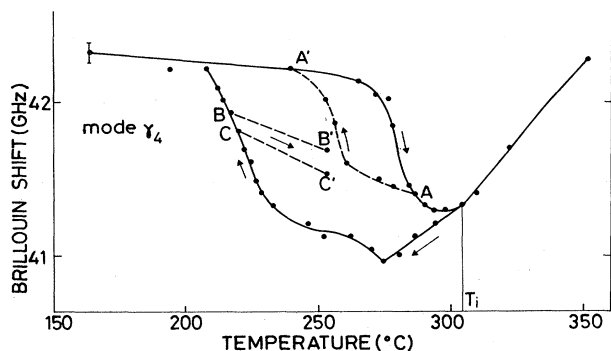
FIG. 6. Temperature dependences of the γ_4-mode frequency measured on various thermal hysteresis cycles. Solid lines: variations related to a heating-cooling cycle between 20 and 450 °C; AA', BB', CC' dashed lines: variations observed after an inversion of the temperature trend at points A, B, and C.

In a second type of experiment, we kept the sample temperature fixed (between 250 and 300 °C) and looked for a time evolution of the Brillouin spectra over several days. We could only observe in some of these experiments a small shift (~ 160 MHz) of the γ_1- and γ_4-mode frequencies lying within the limit of the experimental uncertainties (± 80 MHz). Hence, an improvement of the accuracy of our measurements would be needed to confirm the direct observation of a relaxation effect in the elastic properties of BSN.

However, such a relaxation can be indirectly revealed by the occurrence of a "memory" effect. In a third experiment, after a 24-h annealing of the sample at 275 °C (A point of Fig. 7, left side), we observed the temperature dependence of the γ_1-mode frequency on a cooling run down to 20 °C followed by a heating run up to 270 °C. The variations of this frequency do not follow the usual solid $ABCBD$ curve shown in Figs. 2 and 7(a), but the dashed $A'B'CD'E'$ curve. Hence, the elastic properties of the investigated sample have been modified by the annealing at 275 °C. In particular, the anomalies relative to the B and D points occurred some 20 °C below.

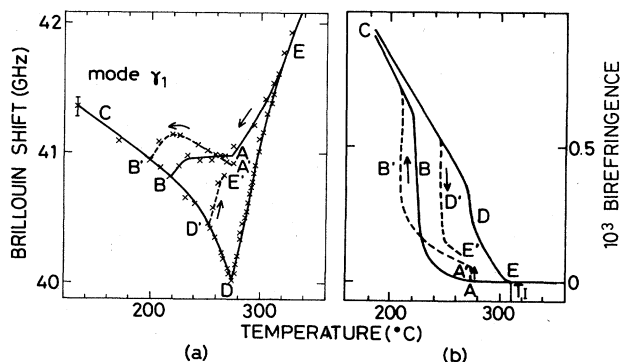Such a behavior confirms the observations carried out

with a similar procedure on the spontaneous birefringence[6] of BSN [Fig. 7(b)]: relaxation inside the INCP induces an increase of the stability range of this phase and therefore a decrease of the lock-in transition temperatures. The comparison between the results of Figs. 7(a) and 7(b) shows that the same phenomena are observed in both cases.

Though they are not exhaustive, all these results are sufficient to demonstrate that the interaction between the incommensurate modulation and the defects revealed by x-rays and birefringence measurements strongly influences the elastic properties of BSN as well.

3. Other modes

The temperature dependences of the frequencies of the other investigated acoustic modes are plotted in Fig. 8. The behavior of the longitudinal γ_{10}-mode frequency looks like those of the γ_4 mode, but with smoother variations in the stability range of the INCP. Its thermal hysteresis has not been investigated. The frequencies of the γ_3, γ_5, γ_{11}, and γ_{12} transverse modes are nearly constant and equal between 20 and 500 °C. We do not detect any anomaly at the transitions. We could not measure the intrinsic linewidth of all these modes since their apparent linewidths are always equal to the instrumental resolution (1.2 or 0.8 GHz).

However, the identification of the γ_{11} mode in the $x(y,z)y$ Brillouin spectra is questionable. Actually, the selection rules given by Vacher and Boyer[24] indicate that this mode is inactive in the tetragonal phase, while we observed it with comparable intensities in all three phases. This problem—which does not seem to be related to the incommensurate feature of the investigated transitions
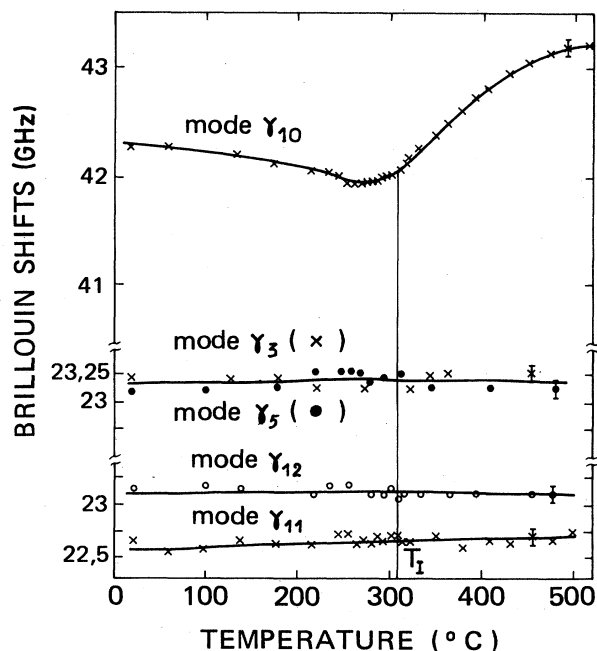

FIG. 7. Comparison between the measurements of the γ_1-mode frequency (on left) and the spontaneous birefringence (on right). Solid lines: temperature dependences of both quantities on a heating-cooling cycle. Dashed lines: variations after a 24-h anneal at 275 °C (A point).

FIG. 8. Temperature dependences of the γ_3-, γ_5-, γ_{10}-, γ_{11}-, and γ_{12}-mode frequencies.

(since the γ_{11}-mode observation only violates the rule selection in the NP)—has been discarded.

Besides these acoustic modes, we also observed another excitation on all the (zz) Brillouin spectra obtained when the incident and scattered electric fields were polarized along the [001] directions. Actually, the background of these spectra is not frequency dependent, but its intensity is much larger than the value (5 cps) we can estimate from the known contrast of the Fabry-Perot interferometer (see Fig. 2). It increases from about 25 to 1000 cps between 20 °C and $T_f = 580$ °C (the ferroelectric transition temperature of BSN) and rapidly falls down above 580 °C, in the paraelectric phase. A preliminary Raman scattering study[22] has shown that this signal can be attributed to the low-frequency responses of two different excitations: an amplitude mode related to the INCP and the soft mode of the ferroelectric transition. By contrast, no signal has been detected which can be assigned to a phase mode.

B. Sound velocities and elastic constants

The sound velocities of the observed acoustic modes and the isothermal and adiabatic elastic constants of BSN have been calculated as explained in Sec. II. Their values at 20, 309 (in the normal phase), and 450 °C are listed in Table III.

The temperature dependences of the adiabatic and isothermal C_{11}, C_{22}, $\widetilde{C}_{11}$, C_{44}, and C_{55} elastic constants (at fixed electric field) are plotted in Fig. 9. C_{44} and C_{55}, which are not affected by the isothermal-adiabatic correction, present an anomaly neither at the LIT nor the NIT. The variations of C_{11}^S, C_{22}^S, and $\widetilde{C}_{11}^S$ look like those of the frequencies of the γ_1, γ_4, and γ_{10} modes (Figs. 3 and 8),

FIG. 9. Temperature dependences of the adiabatic (on left) and isothermal (on right) elastic constants.

TABLE III. Sound velocities and adiabatic and isothermal elastic constants of BSN at 20, 309 (in the normal phase), and 479 °C. The meaning of the γ_i notation is given in Table II and in Ref. 24.

	20 °C	309 °C	479 °C
	Sound velocities (m/s)		
γ_1	6741±12	6591±18	6770±18
γ_3	3643±6	3620±9	3580±9
γ_4	6842±12	6591±18	6770±18
γ_5	3601±6	3627±9	3582±9
γ_{10}	6809±12	6697±18	6754±18
γ_{11}	3649±12	3617±9	3549±18
γ_{12}	3631±12	3619±9	3576±9
	Elastic constants (10^9 N/m^2)		
C_{11}^S	241±1	228±1	240±1
C_{11}^T	236±1	225±1	238±1
C_{22}^S	248±1	228±1	240±1
C_{22}^T	245±1	225±1	238±1
$\widetilde{C}_{11}^S$		237±1	241±1
$\widetilde{C}_{11}^T$		235±1	239±1
$C_{44}^S = C_{44}^T$	66.5±0.5	66.5±0.5	66.5±0.5
$C_{55}^S = C_{55}^T$	66.5±0.5	66.5±0.5	66.5±0.5

except above 430 °C, where these elastic constants decrease. This softening is related to the existence of the ferroelectric transition of BSN at 580 °C. This effect is not apparent on the variations of the frequencies, since for these quantities it is compensated for by the relatively large increase of the n_c refractive index.[20]

As discussed in the last section, the adiabatic-isothermal correction is slowly temperature dependent in the NP and in the QCP. Therefore the variations of C_{11}^T, C_{22}^T, and $\widetilde{C}_{11}^T$ nearly reproduce those of the respective adiabatic constants in both phases. In the INCP, because of the large uncertainty on the adiabatic correction, the variations of C_{11}^T and of C_{22}^T cannot be determined with good accuracy. On the basis of the dilatometric measurements of Abell,[26] it seems that these constants do not undergo jumps either at the NIT or the LIT. Besides, it is possible that the slight anomalies, observed on the variations of C_{11}^S and of C_{22}^S, at, respectively, 220 and 275 °C on cooling runs, are not intrinsic features of the isothermal elastic properties of BSN, but are induced by the anomalous behavior of the expansion coefficients.

Our results can be compared to those previously available for BSN. On one hand, the room-temperature values of the adiabatic elastic constants (at constant electric field) C_{11}, C_{22}, C_{44}, and C_{55} measured by Warner,[27] Yamada,[20] and Busch[19] are listed in Table IV. They are in good agreement with ours. The slight discrepancies can probably be attributed to composition differences of the non-stoichiometric samples investigated. On the other hand, the temperature dependences of the γ_1- and γ_4-mode sound velocities and of the related Brillouin linewidths have been measured by Young and Scott at various frequencies (5.6, 45, and 63 GHz). The measurements performed at 45 GHz qualitatively resemble those obtained here for the heating runs, but with smaller variations of the velocities and linewidths in the INCP. However, these authors do not specify their measuring procedure, the importance of which we have stressed above, nor the sample composition, so that their data cannot be clearly analyzed.

IV. THE LANDAU THEORY OF THE ELASTIC ANOMALIES OF BSN

Let us now discuss these experimental results from a phenomenological point of view.

The most natural step consists in the derivation of the

TABLE IV. Comparison between the measurements of several adiabatic elastic constants.

Authors	References	Experimental technique	$C_{11}^{E,S}$	$C_{22}^{E,S}$	$C_{44}^{E,S}$	$C_{55}^{E,S}$
					(10^9 N/m^2)	
Warner	27	Electromechanical resonance	239	247	65	66
Yamada	20	Electromechanical resonance			70	71.4
Busch	19	Brillouin scattering (6328 Å)	245	258	68.5	64.7
Errandonea	This work	Brillouin scattering (5145 Å)	241±1	248±1	66.5±0.5	66.5±0.5

anomalies of the elastic constants of pure BSN (without defects) in the framework of the Landau theory in a formulation adapted to incommensurate transitions.[31] The explicit form of the BSN free-energy expansion as well as its qualitative consequences on its static properties have already been given by Toledano et al.[34] and Schneck et al.[3] In this section, first, we shall recall their main results. Second, we shall study the temperature dependences of the elastic constants, with special emphasis on the coupling between the amplitude and the wavelength of the modulation near the LIT. Third, the predictions of the Landau theory will be compared to the experimental results.

A. Static and elastic properties

Following Toledano[34] and Schneck,[3] the OP of the BSN incommensurate transition has four components ρ, ϕ and ρ', ϕ', respectively, related to the wave vectors $\pm \mathbf{k}_i$ and $\pm \mathbf{k}'_i$:

$$\mathbf{k}_i = (1+\delta) \left[\frac{\widetilde{\mathbf{a}}^* + \widetilde{\mathbf{b}}^*}{4} \right] + \frac{\mathbf{c}^*}{2} ,$$

$$\mathbf{k}'_i = (1+\delta) \left[\frac{\widetilde{\mathbf{a}}^* - \widetilde{\mathbf{b}}^*}{4} \right] + \frac{\mathbf{c}^*}{2} .$$
(6)

In the reference frame constituted by the principal crystallographic axes of the orthorhombic phase, the free energy is

$$F = \int (f_1 + f_2 + f_3) dv ,$$
(7)

where

$$f_1 = \frac{\alpha}{2}(\rho^2 + \rho'^2) + \frac{\beta_1}{4}(\rho^4 + \rho'^4) + \frac{\beta_2}{4}[\rho^4 \cos(4\phi) + \rho'^4 \cos(4\phi')] + \frac{\beta_3}{2}\rho^2\rho'^2 + \lambda \left[\rho^2 \frac{\partial \phi}{\partial x} + \rho'^2 \frac{\partial \phi'}{\partial y} \right]$$

$$+ K_1 \left[\rho^2 \left[\frac{\partial \phi}{\partial x} \right]^2 + \left[\frac{\partial \rho}{\partial x} \right]^2 + \rho'^2 \left[\frac{\partial \phi'}{\partial y} \right]^2 + \left[\frac{\partial \rho'}{\partial y} \right]^2 \right] + K_2 \left[\rho^2 \left[\frac{\partial \phi}{\partial y} \right]^2 + \left[\frac{\partial \rho}{\partial y} \right]^2 + \rho'^2 \left[\frac{\partial \phi'}{\partial x} \right]^2 + \left[\frac{\partial \rho'}{\partial x} \right]^2 \right]$$

$$+ K_3 \left[\rho^2 \left[\frac{\partial \phi}{\partial z} \right]^2 + \left[\frac{\partial \rho}{\partial z} \right]^2 + \rho'^2 \left[\frac{\partial \phi'}{\partial z} \right]^2 + \left[\frac{\partial \rho'}{\partial z} \right]^2 \right] ,$$
(8)

$$f_2 = \tfrac{1}{2} \sum_{i,j=1}^{3} C_{ij}^0 e_i e_j + \tfrac{1}{2} \sum_{k=4}^{6} C_{kk}^0 e_k^2 ,$$
(9)

$$f_3 = (\rho^2 - \rho'^2) \left[\frac{m_1 - m_2}{2}(e_1 - e_2) + \frac{m_4 - m_5}{2}(e_4^2 - e_5^2) \right]$$

$$+ (\rho^2 + \rho'^2) \left[\frac{m_1 + m_2}{2}(e_1 + e_2) + m_3 e_3 + \frac{m_4 + m_5}{2}(e_4^2 + e_5^2) + m_6 e_6^2 \right] .$$
(10)

f_1 is the usual free-energy expansion related to the bare OP. f_2 is the elastic energy in the form adapted to the quadratic phase (but referred to the orthorhombic axes). f_3 contains the lowest-order coupling terms between the strains and the OP components.

Among the various solutions[34] minimizing F, the case realized in BSN corresponds to the freezing, in the INCP, of one pair of OP components, i.e., to either of the conditions $(\rho \neq 0, \rho' = 0)$ or $(\rho = 0, \rho' \neq 0)$ which, respectively, define two domains with mutually perpendicular modulation directions. This case occurs if we assume that

$$\beta_3 + 2 \sum_{i,j=1}^{3} s_{ij}^0 m_i m_j > \beta'_1 > |\beta_2|$$

and
(11)

$\beta_2 < 0$,

where

$$\beta_1' = \beta_1 - 2 \sum_{i,j=1}^{3} s_{ij}^0 m_i m_j$$

and   (12)

$$(s_{ij}^0) = (c_{ij}^0)^{-1} \quad (i,j=1,\ 2,\ \text{or } 3) ,$$

in addition to the usual conditions

$$\alpha = a(T - T_0) , \quad a, K_1, K_2, K_3 > 0 .$$ (13)

The striking characteristics of the coupling between the OP and the strain components, which plays the prominent part in the specific mechanical properties (strains, elastic constants) of BSN, is that the strains are only coupled to the moduli of the OP and not to their phases. Therefore, below the NIT (where $\rho \neq \rho'$), the macroscopic symmetry of BSN is broken through the onset of a spontaneous value for $(e_1 - e_2)$, and an orthorhombic symmetry is established both in the INCP and QCP. This situation contrasts with the cases of all the other incommensurate phases studied up to now[5] for which the average point symmetry of the INCP was identical to that of the high-temperature phase.

Within the phase-modulation-only (PMO) approximation[31] (homogeneous moduli), the derivation of the static properties from the free energy (7)—(13) leads to a situation similar to that of a two-component OP, which has been thoroughly investigated by various authors.[31−33] Therefore, the standard sequence of events predicted for an INCP with a two component OP [variations of $\delta(T)$,

modulation shape, LIT characteristics] remains valid for BSN.[3]

B. Elastic anomalies

As shown in the Appendix, the temperature dependences of the elastic constants can be deduced from the variations of the OP amplitude ρ through the relations (A7) and (A12). The derivation of these dependences is straightforward in the three phases (NP, INCP, and LP), except just above the LIT. Actually, in this temperature range the free-energy minimization equations cannot be rigorously solved, even in the PMO approximation. Moreover, De Pater et al.[35] showed that the characteristics of the solution strongly depends upon the way the coupling between ρ and the modulation wave vector q is handled. Hereafter, we shall consider three successive steps of approximation leading to different temperature dependences of the elastic constants above the LIT.

(a) As a first approximation, we may neglect this coupling. In this case the LIT is continuous and ρ smoothly varies above the LIT according to the same law in the locked phase. The temperature dependences of ρ, q, and the elastic constants in the three phases are given in Table V and are schematically plotted in Fig. 10 with solid lines.

The elastic behavior at the NIT looks like that obtained for an ordinary structural transition of the improper ferroelastic type[36] (characterized by $\rho^2 e_i$ and $\rho^2 e_k^2$ coupling terms as in BSN); hence, the incommensurate nature of BSN does not induce any specific elastic behavior at the NIT. At the LIT the elastic constants behave above T_L as in the LP and do not undergo any anomaly.

(b) As a second step of approximation, we take into account the coupling between ρ and q. In this case numeri-

TABLE V. Theoretical expressions of the modulation wave vector q, OP amplitude ρ, and elastic constants of BSN derived in the framework of the Landau theory, within the phase-modulation-only approximation. We get $T_i = T_0 + \lambda^2/aK_1$ and $T_L' > T_L = T_0 + (\pi^2/8)(1 + \beta_1'/\beta_2)(\lambda^2/aK_1)$. The other coefficients are defined in the free-energy expansions (7)—(15).

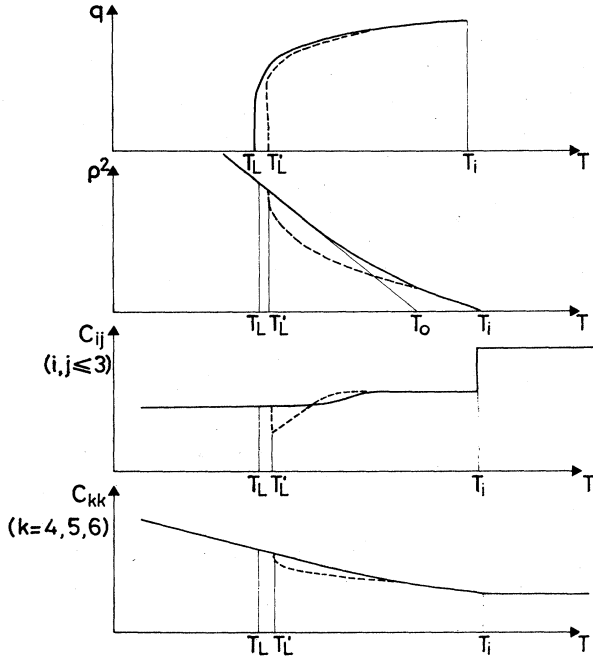|	Normal phase	Incommensurate phase			Locked phase
		Near the NIT	Near the LIT		
			Approximation (a)	Approximation (b)	
	$T \geq T_i$	$T \lesssim T_i$	$T \gtrsim T_L$	$T \gtrsim T_L'$	$T \leq T_L$ or $T \leq T_L'$
q		$-\dfrac{\lambda}{2K_1}$	$\propto [\ln(T-T_L)]^{-1}$	$\propto [\ln(T-T_L)]^{-1}$	0
ρ^2	0	$\dfrac{a(T_i-T)}{\beta_1'}$	$\dfrac{a(T_0-T)}{\beta_1'+\beta_2}$	$\dfrac{a(T_0-T)}{\beta_1'+\beta_2}$ $-\dfrac{Aq[a(T_0-T)]^{1/2}}{(\beta_1'+\beta_2)^{3/2}}$	$\dfrac{a(T_0-T)}{\beta_1'+\beta_2}$
C_{ij} $(i,j=1,2,3)$	C_{ij}^0	$C_{ij}^0 - \dfrac{2m_i m_j}{\beta_1}$	$C_{ij}^0 - \dfrac{2m_i m_j}{\beta_1+\beta_2}$	$C_{ij}^0 - \dfrac{2m_i m_j}{2\sum s_{ij}^0 m_i m_j}$ $-u[\ln(T-T_L)]^2$	$C_{ij}^0 - \dfrac{2m_i m_j}{\beta_1+\beta_2}$
C_{kk} $(k=4,5,6)$	C_{kk}^0	$C_{kk}^0 + \dfrac{am_k(T_i-T)}{\beta_1'}$	$C_{kk}^0 + \dfrac{am_k(T_0-T)}{\beta_1'+\beta_2}$	$C_{kk}^0 + \dfrac{am_k(T_0-T)}{\beta_1'+\beta_2}$ $-m_k\dfrac{Aq[A(T_0-T)]^{1/2}}{(\beta_1'+\beta_2)^{3/2}}$	$C_{kk}^0 + \dfrac{am_k(T_0-T)}{\beta_1'+\beta_2}$

FIG. 10. Qualitative temperature dependences of the modulation wavevector, the OP amplitude, and the elastic constants of BSN calculated within the phase-modulation-only approximation. Solid lines correspond to the approximation (a) defined in the text, dashed lines to approximation (b).

cal calculations of de Pater[35] show that a discontinuous LIT occurs at a temperature T_L' slightly higher than T_L, and that ρ_s takes smaller values than in the preceding case.

Approximate algebraic expressions of the temperature dependences of ρ_s, q, and the elastic constants can be found in the vicinity of the LIT, with the help of the soliton formalism introduced by Bak and Emery.[37] After elimination of the strains, the BSN free energy can be written in the PMO approximation as

$$\widetilde{F}(\rho,q) = \frac{\alpha\rho^2}{2} + \frac{\beta_1' + \beta_2}{4}\rho^4 + \lambda q\rho^2$$
$$+ A\rho^3 q \left[1 + 4\exp\left[\frac{2\beta_2\rho}{A}\frac{\rho}{q} \right] \right], \qquad (14)$$

with

$$A = \frac{(-8K_1\beta_2)^{1/2}}{\pi}. \qquad (15)$$

A linearization of the minimization equations about the solution found in approximation (a), leads to the temperature dependences shown in Table V and sketched with dashed lines in Fig. 10. In this case, the variations of q induce anomalies on the behavior of ρ and of the elastic constants: the steeper the decrease of q above the LIT, the larger the softening and the jump of C_{ij} constants (i and $j = 1$, 2, or 3) at T_L'.

(c) The above results have been derived within the PMO approximation. The consequences of a spatial modulation of the amplitude cannot be determined so easily since one

can no longer find analytical solutions of the minimization equations. However, it is possible to qualitatively examine the influence of terms in the free-energy expansion, such as

$$\delta F' = \int dv \left[K_1 \left[\frac{\partial\rho}{\partial x} \right]^2 + \mu\rho^2 \left[\frac{\partial\rho}{\partial x} \right]^2 \right]. \qquad (16)$$

So far, we have not considered the last term of this expression in the expansion (7)—(10). Ishibashi,[38] Durand,[39] and Lederer[40] and co-workers showed up its essential role to explain some properties of $NaNO_2$ and $SC(NH_2)_2$. Its coefficient μ is positive because of stability conditions.

The gradient terms in (16) induce an additional cause of coupling between the amplitude and the wavelength of the modulation which we did not consider before. The quantity $\delta F'$ is positive and increases with q, the modulation wave vector. Hence, $\delta F'$ reduces the stability of the INCP: the LIT occurs at a temperature T_L'' higher than T_L' and T_L. It is likely to be discontinuous, as shown by the numerical calculations of Ishibashi and Shiba.[38] Secondly, the minimum of the free energy $F + \delta F'$ at a fixed temperature occurs for a lower value of q than that of the homogeneous amplitude case. Ishibashi and Shiba show that q undergoes a more regular decrease throughout the INCP than the usual pathological logarithmic law. As a consequence, the variations of the OP amplitude are smoother than in the PMO approximation, and the softening of the C_{ij} constants is reduced.

In summary, a Landau theory of the incommensurate transitions of BSN leads one to expect the following features:

(1) The elastic properties of BSN are determined by the temperature dependence of the modulation amplitude ρ_s. Relations (A7) and (A12) hold even if the PMO approximation is released.

(2) On cooling, the elastic constants C_{ij} (i and $j = 1$, 2, or 3) undergo a downward jump at the NIT, a softening in the INCP, and an upward jump at the LIT. The variations of the constant C_{kk} ($k = 4$, 5, or 6) are continuous at both transitions, but exhibit slope changes. In the PMO approximation, the amplitudes of these anomalies are listed in Table V. If we release this approximation, the magnitude of the anomalies and the stability of the INCP are reduced.

C. Discussion

Let us compare our experimental data with the preceding theoretical results.

The measured elastic constants C_{44} and C_{55} do not exhibit any anomaly either at the NIT or the LIT (Fig. 9). This behavior is consistent with the Landau theory if the coupling coefficients m_4 and m_5 between ρ, e_4, and e_5 are so small that the expected amplitudes of the anomalies of C_{44} and C_{55} are within the experimental uncertainties. Taking $\Delta C_{44} = \Delta C_{55} = \pm 0.5 \times 10^9$ N/m^2 and $\rho^2 = 5 \times 10^{-19}$ kg m^{-1} at 20 °C (see Table VII), we find

$$m_4 \text{ and } m_5 \leq 10^{27} \text{ s}^{-2}. \qquad (17)$$

By contrast, the predictions of the Landau theory for

C_{11} and C_{22} only very roughly account for their measured temperature dependences (Fig. 9). From a qualitative point of view, three features of the experimental variations are in disagreement with the Landau theory: the rounding of $C_{11} = C_{22}$ in the normal phase, the absence of jumps at the NIT and the LIT, and the large thermal hysteresis in the 200–300 °C temperature range. (The hardening of C_{11} and C_{22} in the locked phase can be explained by the introduction of terms of degree higher than four in the free-energy expansion.) Therefore, we need to consider several effects which are not taken into account by the above theory to obtain a better description of the behavior of C_{11} and C_{22}. This is the purpose of the next two sections.

V. EFFECT OF THE CRITICAL FLUCTUATION OF THE OP ABOVE T_i

In this section we quantitatively show that the elastic anomalies in the high-temperature phase (namely, the rounding of C_{11} and the decrease of the related Brillouin linewidth) can be induced by the thermodynamic critical fluctuations of the OP. (We shall not consider the influence of the defects,[41] which can sometimes have an effect similar to the thermodynamic fluctuations.)

The most simple treatment of the effect of the OP fluctuations of a displacive phase transition on the acoustic properties was first given by Levanyuk[42] within the mean-field approximation, by solving the motion equations of the coupled soft-optic—acoustic-mode system, one degree of approximation beyond the usual linear approximation.

This theory has been applied by Yao et al.[43] in the case of terbium molybdate (TMO), which is very similar to ours. Actually, neither the incommensurate nature of the OP nor its dimensionality (2 for TMO, 4 for BSN) play a specific role in the derivation of the elastic anomalies induced by the fluctuations. A straightforward calculation, starting from the BSN free energy (7)–(10) and closely following the line of the method of Yao et al., leads to the following results for the γ_1 mode above T_i:

$$C_{11}(\mathbf{q},\omega) = C_{11}^0 - \frac{16}{(2\pi)^7}(m_1^2 + m_2^2)k_B T$$
$$\times \int \frac{d\mathbf{Q}}{4\Omega^4(\mathbf{Q}) + \omega^2\Gamma^2(\mathbf{Q})} , \qquad (18)$$

$$\gamma(\mathbf{q},\omega) = \gamma_0 + \frac{8}{(2\pi)^7}\frac{q^2}{\rho}(m_1^2 + m_2^2)k_B T$$
$$\times \int \frac{\Gamma(\mathbf{Q})d\mathbf{Q}}{\Omega^2(\mathbf{Q})[4\Omega^4(\mathbf{Q}) + \omega^2\Gamma^2(\mathbf{Q})]} , \qquad (19)$$

where γ_0 is the bare damping coefficient related to the γ_1 mode in the absence of coupling between the strains and the OP, $\mathbf{q}$ and ω are the respective wave vector and frequency of the investigated acoustic mode, and $\Omega(\mathbf{Q})$ and $\Gamma(\mathbf{Q})$ are the frequency and the damping coefficient of the optic mode belonging to the soft-mode branch. The triple integration is performed in the Brillouin zone of the quadratic phase.

These equations show that the knowledge of the soft-optic-mode dispersion curve allows the determination of the fluctuations' contribution to the elastic anomalies. Because of the presence of Ω^4 and Ω^6 terms in the denominators, this contribution increases rapidly in the prototype phase close to the transition when the optic branch softens. It induces a downward bending of the elastic constants as well as an increase of the damping coefficients.

A. Data analysis

Equations (18) and (19) have been used to analyze the elastic properties of the γ_1 mode in the prototype phase.

The characteristics of the soft-optic dispersion curve of BSN can be deduced from the neutron scattering data of Schneck et al.[3] Though their measurements are not complete in this aspect, they are sufficient to calculate the values of both integrals. Actually, these values are not sensitive to the details of the dispersion curve except to the form of this curve in the vicinity of its minimum which occurs at the incommensurate wave vector $\mathbf{k}_i$. However, a difficulty arises from the fact that the soft-optic branch interacts with a central mode. Hence, the apparent frequencies $\Omega_\infty(\mathbf{Q})$ and linewidths $\Gamma_\infty(\mathbf{Q})$, measured by Schneck et al., are renormalized by this frequency-dependent interaction and are not the effective frequencies $\Omega(\mathbf{Q})$ and linewidths $\Gamma(\mathbf{Q})$ appearing in Eqs. (18) and (19). Neglecting a direct coupling between the central mode and the γ_1 mode, we assume, as usual for an optic-mode—central-mode coupled system,[44] that the effective optic frequencies and damping coefficients are given by

$$\Omega^2 = \Omega_\infty^2 - \frac{\Delta^2}{1 + \omega^2\tau^2} , \qquad (20)$$

$$\Gamma = \Gamma_\infty + \frac{\Delta^2\tau}{1 + \omega^2\tau^2} , \qquad (21)$$

where Δ is the strength of the coupling, ω is the Brillouin frequency of the γ_1 mode, and τ is the characteristic relaxation time of the bare central mode.

Besides, we also need to know the background elastic constant C_{11}^0 in the absence of coupling to the soft mode. Owing to the presence of the ferroelectric transition of BSN at $T_f \sim 580$ °C, we cannot consider that C_{11}^0 slowly decreases on heating as usual.[43] We assume that the longitudinal strains and the ferroelectric polarization P are coupled through a term $\sum_i \eta_i e_i P^2$, where η_i measures the strength of the coupling. Hence, the temperature dependence of the elastic constant C_{11}^0 below T_f is given by

$$C_{11}^0(T) = C^0 - \frac{4\eta_1^2 P^2(T)}{\Omega_p^2} = C^0 - \frac{4NP^2(T)}{\Omega_p^2/\gamma_p} , \qquad (22)$$

with

$$N = \eta_1^2/\gamma_p . \qquad (23)$$

C^0 is the bare elastic constant, and Ω_p and γ_p are the frequency and the damping coefficient of the overdamped ferroelectric soft mode.[45]

The parameters $\Omega_\infty(\mathbf{Q},T)$, $\Gamma_\infty(\mathbf{Q},T)$, and $\Delta(\mathbf{Q},T)$ have been deduced from the neutron data of Schneck,[3] $P_s(T)$

TABLE VI. Values of the various parameters used to fit the variations of C_{11} and γ_1 above the NIT. The experimental wave-vector and temperature dependences of Ω_∞, Γ_∞, and Ω_p^2/γ_p have been fitted to the empirical laws listed below. In these expressions, the components of the wave vector $\mathbf{Q}$ are referred to the quadratic axes. $\Omega_\infty(Z)$ is the experimental frequency of the optic mode at the Z point $(0,0,0.5)$ of the Brillouin zone, and $\Omega_0(\mathbf{k}_i)$ the frequency of the bare soft mode at $\mathbf{k}_i$ in the absence of coupling with the central mode. We assume that $\Omega_\infty(\mathbf{Q})$ saturates to a value $\Omega_{\max}$ when the modulus of $\mathbf{Q} - \mathbf{k}_i$ increases. ($\Omega_{\max}$ is the average frequency of the optic mode belonging to the soft surface far from $\mathbf{k}_i$.) Since no neutron data are available, we estimate its value on the basis of the Raman data of Boudou et al. (Ref. 30) by looking for the frequency of the softest optic mode located at the Brillouin-zone center, the symmetry of which (τ_1, τ_4, or τ_5 of the 4mm point group) is compatible with the symmetry of the OP [$\Gamma_1(k_i^*)$ of the $P4bm$ space group]. The wave-vector dependence of $\Delta(\mathbf{Q}, T)$ has been neglected since the interaction of the optical modes with the central mode do not significantly decrease the experimental frequencies $\Omega_\infty(\mathbf{Q})$, except in the vicinity of $\mathbf{k}_i$. The uncertainties on the fitted values of the free parameters correspond to a degradation of the quality of the fit by a factor of 2, according to the least-squares criterion.

Fixed parameters	Experimental data	Reference
$\Omega_\infty(\mathbf{Q}, T) =$	$\begin{cases} \Omega_\infty(\mathbf{k}, T) + [\Omega_\infty(Z) - \Omega_\infty(\mathbf{k}, T)]\sin^2\left[\dfrac{2}{1+\delta}\dfrac{Q_x^2 + Q_y^2}{a_t^*} - 1\right] \\ + 0.78\left[\dfrac{Q_y - Q_x}{a_t^*}\right]^2 + 33.5\left[\dfrac{Q_z^2}{c^*} - \dfrac{1}{2}\right]^2 \\ \text{when the quantity is smaller than } \Omega_{\max}, \\ \Omega_{\max} \quad \text{otherwise.} \end{cases}$	3
	with	
	$\Omega_\infty^2(\mathbf{k}_i, T) = \Omega_0^2(\mathbf{k}, T) + \Delta^2(\mathbf{k}_i, T)$	
	$\Omega_0^2(\mathbf{k}_i, T) = 1.5 \times 10^{-3}(T - T_I)$ Thz^2	
	$\Delta^2(\mathbf{Q}, T) = 0.125 \exp[-(T - T_i)/90]$ THz^2	
	$\Omega_\infty^2(Z) = 1.1$ Thz, $\Omega_{\max} = 1.45$ GHz	30
	$T_I = 309\,°\mathrm{C}$	
	$a_t^* = \dfrac{2\pi}{12.48}$ Å^{-1}, $c^* = \dfrac{2\pi}{4}$ Å^{-1}, $\delta = 0.12$	
$\Gamma_\infty(\mathbf{Q}, T)$	0.65 Thz	3
$P_s(T)$	$[(0.267 + 0.0064(T_f - T)^{1/2}]$ Cb/m^2, $T_f = 580\,°\mathrm{C}$	15
$\dfrac{\Omega_p^2}{\gamma_p}$	$3.43(T_f - T)$ Ghz	45

Free parameters	Fitted values
$2\pi\tau$	$(16.5 \pm 3) \times 10^{-12}$ s
C_0	$(254 \pm 3.5) \times 10^9$ N m^{-2}
M	$(2 \pm 0.45) \times 10^{53}$ s^{-4}
N	$(8.3 \pm 2) \times 10^{21}$ N^2 m^4 Cb^{-4} s^{-1}
γ_0	(80 ± 30) MHz

from the polarization measurements of Singh,[13] and Ω_p^2/γ_p from the Raman data of Errandonea.[45] Their values are listed in Table VI. The other coefficients—τ,

C^0, $M = m_1^2 + m_2^2$, N, and γ_0—are taken as free parameters whose values must be fitted to account for the experimental data.
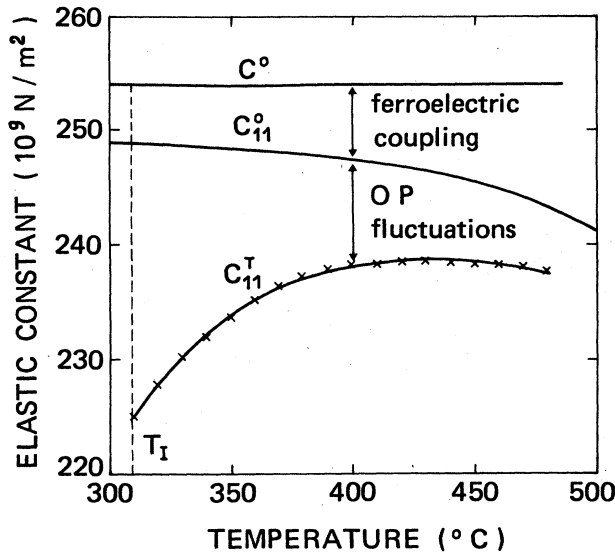
FIG. 11. Temperature dependence of C_{11}^T in the normal phase. Crosses: experimental measurements. Solid line: theoretical fit to formula (17). C^0 and C_{11}^0 are the background elastic constants defined in the text.

We show in Fig. 11 the best fit (using the values of the first four free parameters given in Table VI) to the measurements of the isothermal elastic constant C_{11}^T (performed on an heating run) obtained by a least-squares method. The variations of the background values C^0 and C_{11}^0 are also plotted on this figure. On heating from T_i to 480°C, the fluctuations' contribution decreases from 24×10^9 to 6×10^9 N/m^2, while the ferroelectric contribution increases from 4.9×10^9 to 10.6×10^9 N/m^2. A comparison with the results of Yao shows that the ratio of the fluctuations' contribution at T_i to the background value C_0 is 3 times larger in TMO (27%) than in BSN (9.4%). This quantitative difference can be explained if one notices that the soft dispersion curve is more anisotropic in BSN than in TMO. In particular, the curvature along the [001] direction is very pronounced in BSN (see Table VI), so that there is a small contribution of the fluctuations whose wave vector is parallel to [001]: the relevant fluctuations are quasi-two-dimensional (except very close to T_i).

We also examined the influence of the various physical parameters, which define the form of the soft dispersion curve, on the values of the free parameters. As mentioned above, the values of the fluctuation integrals in (18) and (19) do not depend significantly on the curvature coefficients or on the frequencies $\Omega_\infty(Z)$ and Ω_{max}. A 10% variation of these coefficients induces a variation of the fitting parameters smaller than 1%. By contrast, the parameters which determine the value of the effective minimum frequency $\Omega_0(\mathbf{k}_i, \omega)$ of the soft dispersion curve have a much larger influence on the results, mainly on M and τ. However, their variations always stay in the uncertainty range given in Table VI as long as the variations of $\Omega_0(\mathbf{k}_i, \omega)$ are smaller than 20%.

Let us now examine the temperature dependence of the width of the γ_1 mode in the quadratic phase. The integral

in Eq. (19) has been calculated using the above-fitted values of M and τ. We have corrected the theoretical value thus obtained by taking into account the broadening introduced by the convolution between the intrinsic linewidth and the instrumental response: we assume that the experimental linewidth is given by

$$\gamma_{expt} = (\gamma^2 + \gamma_{res}^2)^{1/2}, \tag{24}$$

where γ is the damping coefficient given by (19) and $\gamma_{res} = 1.2$ GHz is the instrumental linewidth. The experimental data can therefore be fitted directly to the γ_{expt} value resulting from Eqs. (19) and (24) with only one free parameter, γ_0, the damping coefficient of the bare γ_1 mode. The best fit, shown in Fig. 12, is obtained for $\gamma_0 = 80 \pm 30$ MHz.

B. Discussion

Among the five free parameters determined above, two, M and τ, can be compared with available experimental data.

First, we can calculate the M coefficient with the help of formula (A2):

$$m_i = -\frac{1}{\rho^2} \sum_{j=1}^{3} C_{ij}^0 e_j. \tag{25}$$

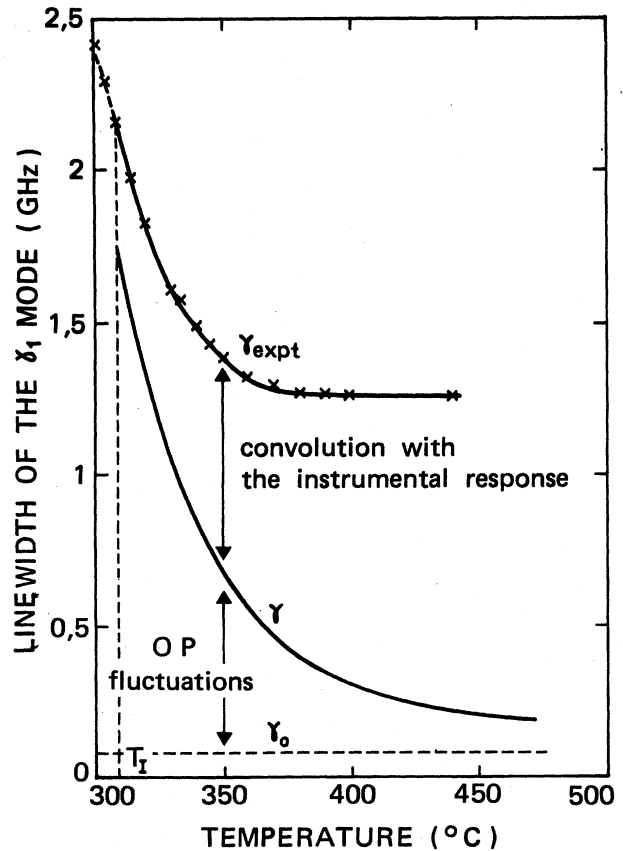Using the values listed in Table VII, we obtain

FIG. 12. Temperature dependence of the linewidth of the γ_1 mode. Crosses: experimental measurements (convoluted with the instrumental response). Solid lines: theoretical fit to Eqs. (18) and (24).

TABLE VII. Values of the parameters used in the numerical calculations of Secs. V and VI.

Elastic constants	$(C_{ij}) = \begin{bmatrix} 239 & 104 & 50 \\ 104 & 245 & 52 \\ 50 & 52 & 135 \end{bmatrix} \times 10^9$ N/m^2	Ref. 27 and Sec. III of this work
Elastic compliances	$(s_{ij}) = \begin{bmatrix} 53 & -19 & -12 \\ -19 & 51 & -12 \\ -12 & -12 & 83 \end{bmatrix} \times 10^{-13}$ N/m^2	Inversion of the (C_{ij}) matrix
Longitudinal strains at 20 °C	$e_1 = (1.2 \pm 0.1) \times 10^{-3}$ $e_2 = -(0.6 \pm 0.1) \times 10^{-3}$ $e_3 \leq 0.4 \times 10^{-3}$	Ref. 26
Order-parameter amplitude	$\rho = 7.07 \times 10^{-10}$ kg$^{1/2}$ m$^{1/2}$ at 20 °C	Ref. 12
Coupling coefficients	$m_1 = (44 \pm 7) \times 10^{25}$ s^{-1} $m_2 = (-4 \pm 10) \times 10^{25}$ s^{-2} $m_3 = (5.8 \pm 10) \times 10^{25}$ s^{-2}	Formula (25)
Other free-energy coefficients	$a = (2\pi)^2 \, 1.5 \times 10^{21}$ k^{-1}s^{-2} $\beta'_1 = 15 \times 10^{42}$ $\beta_1 = 17 \times 10^{42}$	Ref. 3 Table V and Ref. 16 Formula (12)

$$M = m_1^2 + m_2^2 = (2.0 \pm 0.6) \times 10^{53} \text{ s}^{-4}, \quad (26)$$

which matches the above-fitted value very well. This result shows that, in BSN as in gadolinum molybdate,[46] the same m_i coupling coefficients can be used to account for the measurements of three different quantities, namely the expansion coefficients, the elastic constant C_{11}, and the related damping constant γ.

On the other hand, the relaxation time τ can be compared to the measurements of Young and Scott.[21] Actually, these authors, using a scattering-angle-dependent Brillouin experiment, showed a dispersion of the γ_1 mode in the quadratic phase, characterized by a relaxation time (at 45 GHz): $2\pi\tau = (13.5 \pm 2) \times 10^{-12}$ s, while we found $2\pi\tau = (16.5 \pm 3) \times 10^{-12}$ s.

The agreement is convincing since both values have been estimated using very different methods. Besides, the effective optic frequencies used in our approach are frequency dependent [see Eq. (21)] because of their interaction with the central mode. Therefore, our analysis shows that the origin of the dispersion of the γ_1 mode observed by Young and Scott above T_i lies in the indirect coupling of these modes with the central component. Unfortunately, the width of this central peak had not been determined by Schneck[3] because of the lack of resolution (0.15 THz) of the neutron apparatus used. A direct measurement with improved resolution could confirm our analysis.

VI. ACOUSTIC ANOMALIES BELOW T_i

In this section we present a semiquantitative interpretation of the temperature dependences of C_{11} and of C_{22} below the NIT. As has been invoked for several incommensurate materials,[47–50] we consider that the elastic anomalies result from the superposition of two main contributions: a coupling of the acoustic modes with the OP fluctuations and a coupling with the amplitude mode.

However, in BSN these effects are strongly influenced by the defects. Hence, we shall distinguish both contributions in pure BSN crystals (without defects) and in real samples.

A. Elastic anomalies in pure BSN samples

Below T_i the OP-fluctuation contribution is given by an expression similar to (18). However, the integrals in this equation cannot be calculated in the INCP since no experimental data are available on the characteristics of the amplitude mode and of the phase mode. We can only assume that the contributions of the fluctuations relative to C_{11} and to C_{22} are nearly equal and that their magnitude is comparable to the one calculated above T_i. In particular, since the NIT is continuous, we have $(\Delta C_{11})_{fl} = (\Delta C_{22})_{fl} \sim 24 \times 10^9$ N/m^2 close to T_i. On cooling, the frequencies of the soft excitations harden and the fluctuation contributions decrease. Their inferred temperature dependence is schematically plotted on Fig. 13(a).

The contribution of a static coupling with the amplitude mode has been considered in Sec. IV of this paper. However, the strongly overdamped behavior of this excitation[3,22] and the dispersion effects observed by Young and Scott[21] suggest that the static and the dynamic amplitude-mode contributions differ significantly.

Below T_i, the dynamic contribution is given by

$$\Delta C_{ii} = \Delta C_{ii}^0 \frac{1}{1 + \omega^2 \tau_a^2}, \quad (27)$$

where τ_a is the relaxation time of the amplitude mode. The static step anomaly of the Landau theory (see Table V),

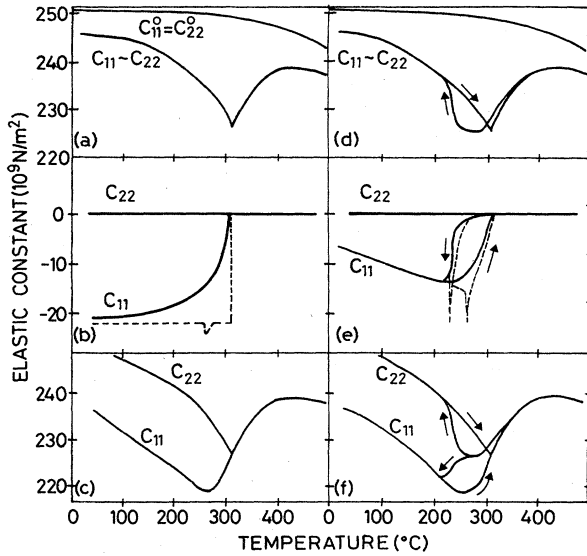$$\Delta C_{ii}^0 = -2 \frac{m_i^2}{\beta_1},$$

FIG. 13. Estimated or calculated temperature dependences of the various contributions to the elastic constants C_{11} and C_{22} in a pure BSN crystal [(a)—(c)] and in a real sample [(d)—(f)]. (a) and (d) represent the variations of the OP fluctuation contribution, (b) and (e) the static (dashed lines) and dynamic (solid lines) responses to the coupling between the amplitude mode and the strains, and (c) and (f) the sum of the various contributions.

is smeared out at the Brillouin frequency ω.

Using the values of Table VII, we obtain

$$\Delta C_{11}^0 = (22 \pm 7) \times 10^9 \text{ N/m}^2 \, ,$$

$$\Delta C_{22} \leq 2 \times 10^9 \text{ N/m}^2 \, . \tag{28}$$

Hence, the amplitude-mode contribution to C_{22} is at least 10 times smaller than the one to C_{11} and can be neglected. To calculate the dynamical variations of C_{11}, one must know the temperature dependence of the amplitude-mode relaxation time. Young and Scott[21] deduced it from their Brillouin measurements of the frequency and of the linewidth of the γ_1 acoustic mode, but they did not take into account the contributions of the fluctuations and the defects. Hence, we have simply assumed instead, according to the Landau-Khalatnikov model,[51] that the dynamic anomaly of C_{11} at 288 °C (the temperature at which the Brillouin linewidth is maximum) is half of the static step.

At the LIT we also assume that the step undergone by the static elastic constant C_{11} (see Sec. IV) is rounded by the dynamic effect, leading to the C_{11} and C_{22} variations shown in Fig. 13(b).

Besides these two main contributions examined above, one may also consider the contributions of the phase mode[52] and high-degree coupling terms between the OP and the strains (such as $\rho^2 e_i^2, \rho^4 e_i, \ldots$). These contributions induce a slight hardening of the elastic constants on cooling which cannot be numerically calculated.

In Fig. 13(c), we have added these various contributions. The resulting variations of C_{11} and of C_{22} resemble those observed for the longitudinal elastic constants of several incommensurate materials: $NaNO_2$,[47] K_2SeO_4,[48] $Sc(NH_2)_2$,[49] etc. In these compounds the related strains

are totally symmetric with respect to the space group of the prototype phase. This is not the case for e_1 and e_2 in BSN, but, because of the unusual symmetry change of this crystal at the NIT, the OP strain-coupling terms have the same form in all these materials, i.e., they do not depend on the OP phase. As a consequence, the same mechanisms as those discussed above can be invoked to explain the elastic anomalies. However, in the case of BSN, this analysis does not provide a complete description of the experimental measurements [compare Figs. 13(c) and 9(a)]: in particular, the temperature dependences of C_{11} and C_{22} on the cooling run is not accounted for. Let us show that the influence of the defects on the elastic properties explains this discrepancy.

B. Influence of the defects

It is now well established that a strong interaction between the incommensurate modulation and some mobile defects plays an important role on the properties of BSN.[6] Its elastic properties are also affected by this interaction: we showed that the C_{11} and C_{22} measurements disclose the existence of a memory effect, and also metastable states, similar to those already observed in the study of the optical birefringence or of diffraction satellites.

To relate, from a phenomenological point of view, the influence of the defects on these different quantities, we shall take into account two main effects induced by the defects and revealed by the birefringence and the satellite measurements: On one hand, a large thermal hysteresis characterized by different transition temperatures on heating ($T_L \sim 270$ °C, $T_i \sim 310$ °C for a heating rate ~ 0.3 °C/min) and on cooling ($T_L \sim 225$ °C, $T_i \sim 290$ °C for the same rate), and on the other hand, a temperature dependence of the OP amplitude different from the behavior expected for a pure system. Actually, in the framework of the Landau theory, we expect a linear temperature dependence in the INCP for the quantities proportional to the OP square, such as the spontaneous birefringence, the spontaneous shear $e_2 - e_1$, or the intensity of the incommensurate satellites. By contrast, the observations[6,16] show that all these quantities increase very slowly below T_i and vanish at the NIT with a horizontal slope (see Fig. 7). This phenomenon is particularly pronounced on cooling.

Let us reexamine both the fluctuations and the amplitude-mode contributions, taking into account these two effects.

First, their temperature dependences are shifted by nearly 20 °C because of the hysteresis on the NIT temperatures. This effect accounts for the thermal hysteresis observed in the NP. Secondly, it is likely that the frequencies of the soft excitations, amplitude mode and phase modes which determine the magnitude of the fluctuations effect in the INCP [formula (18)] increase very slowly below the NIT as the OP amplitude does. Hence the fluctuation integral decreases very slowly below T_i. By contrast, below 290 °C for the heating runs and below 270 °C for the cooling runs, the OP amplitude strongly increases and the fluctuation contributions rapidly vary to become equal near 215 °C (at the end of the hysteresis observed on the birefringence measurements). Its temperature depen-

dence is sketched in Fig. 13(d). Thirdly, in the same manner, the coupling between the amplitude mode and the strain e_1 no longer induces any anomalies at the NIT, but rather at lower temperatures when the OP undergoes large variations. More precisely, the static amplitude-mode contribution can be quantitatively determined with the help of relation (A12), in which $\rho_s(T)$ no longer represents the temperature dependence of the OP amplitude of a pure system in the framework of the Landau theory, but rather the one of a real BSN sample with a large defect concentration. Using the data of Tables V and VII and the birefringence measurements reported in Fig. 7(b), we obtain the static elastic responses plotted with dashed lines in Fig. 13(e). The solid lines represent the dynamic response of the system when we again assume that the rapid variations of the static elastic constant C_{11} at the LIT are smeared out.

In Fig. 13(f), we have added the different contributions influenced by the defects. The theoretical variations of C_{11} and C_{22} thus obtained are now in good agreement with the experimental results. Let us note that a similar analysis can be used to explain the temperature dependence of C_{11} observed after an annealing in the INCP (memory effect). In this case, the temperature dependence of the OP amplitude is changed. With the help of the birefringence data [dashed lines of Fig. 7(b)], we can calculate the new contribution of the coupling between e_1 and the amplitude mode. This procedure leads to the C_{11} variations plotted in Fig. 14, in good agreement with the
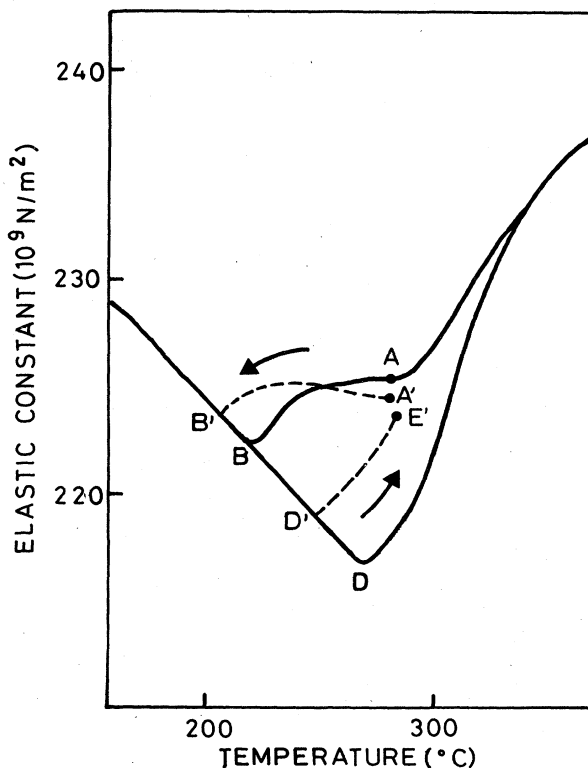

FIG. 14. Calculated temperature dependence of C_{11} on a usual heating-cooling cycle (solid line) or after a 24-h anneal at 275 °C (dashed lines). For a comparison with the experimental measurements, see Fig. 7.

measurements shown in Fig. 7(a).

Therefore, the analysis reported in this section leads to a satisfactory semiquantitative description of the experimental data. It confirms the fundamental influence of the defects on the properties of BSN.

VII. CONCLUSION

In this paper we have reported an experimental and phenomenological study of the elastic properties of incommensurate BSN. The velocities, the linewidths of the main acoustic modes propagating in the (001) plane, and the related elastic constants C_{11}, C_{22}, $\tilde{C}_{11}$, C_{44}, and C_{55} have been measured between 20 and 500 °C in the normal phase, the incommensurate phase, and the quasilocked phase of BSN.

The main anomalies have been observed on C_{11} and on C_{22}. Their form strongly depends on the experimental conditions. In particular, a large thermal hysteresis (~ 100 °C) of a specific type and a memory effect have been described. These effects are similar to those already observed for other properties of BSN, such as the spontaneous optical birefringence, or the satellite characteristics. They have been related to an interaction between the incommensurate modulation and certain mobile defects. A temperature-dependent background has been observed on the totally symmetric Brillouin spectra, which has been assigned to the overdamped amplitude mode, but no effect related to a gapless phase mode has been detected, probably because of the presence of defects interacting with the modulation.

From a theoretical point of view, we have shown that the Landau theory of incommensurate transitions is insufficient to account for the variations of C_{11} and of C_{22}. By contrast, an agreement with the experimental data is obtained when we describe the elastic properties of real BSN samples as the result of the superposition of two types of responses: On one hand, the response of a standard (without defects) incommensurate crystal in which the longitudinal strains are bilinearly coupled to the square of the OP amplitude. In the NP we have quantitatively shown that the rounding of C_{11} ($=C_{22}$) is induced by the OP fluctuations. In the INCP this effect is the main contribution to the variations of C_{22}, while the temperature dependence of C_{11} is also influenced by a dynamical coupling between e_1 and the overdamped amplitude mode. On the other hand, the elastic properties of real BSN samples are strongly influenced by defects. They induce a large thermal hysteresis, an unusual temperature dependence in the INCP, and an extreme sensitivity to the experimental procedure. These anomalies have been quantitatively correlated to the ones observed on the birefringence measurements.

The nature of the involved mobile defects has not yet been identified with certainty. However, on the basis of structural arguments, as well as of birefringence measurements performed on BSN samples with different off-stoichiometry compositions, it seems likely that they have an extrinsic origin, namely they are sodium vacancies. It would be interesting to study the stoichiometry dependence of the elastic properties in order to confirm our analysis.

ACKNOWLEDGMENTS

APPENDIX: RELATIONS BETWEEN THE ELASTIC CONSTANTS AND THE ORDER-PARAMETER AMPLITUDE

In this appendix we derive the relations between the elastic constants and the OP amplitude without the use of the modulation-phase-only approximation. The derivation essentially lies on the fact, specific to BSN, that the elastic strains are not coupled to the OP phases.

The minimization of the Gibbs energy,

$$G = F - \int dv \left[\sum_{i=1}^{6} \sigma_i e_i \right] , \tag{A1}$$

leads to equations of states between the strains, the stresses σ_i, and the OP components in which the OP moduli ρ and ρ' can be decoupled. For one family of ferroelastic domains ($\rho'=0$) with a modulation along the x axis, we obtain

$$\sigma_i = \sum_{j=1}^{3} (C_{ij}^0 e_j) + m_i \rho^2 \quad (i=1, 2, \text{ or } 3) , \tag{A2}$$

$$\sigma_k = (C_{kk}^0 + 2m_k \rho^2)e_k \quad (k=4, 5 \text{ or } 6) , \tag{A3}$$

$$\frac{\partial}{\partial x} \frac{\partial f_1}{\partial(\partial\rho/\partial x)} = \frac{\partial f_1}{\partial \rho} + 2\rho \sum_{i=1}^{3} m_i e_i + 2\rho \sum_{k=4}^{6} m_k e_k^2 , \tag{A4}$$

$$\frac{\partial}{\partial x} \frac{\partial f_1}{\partial(\partial\varphi/\partial x)} = \frac{\partial f_1}{\partial \varphi} , \tag{A5}$$

with

$$f_1 = \frac{\alpha\rho^2}{2} + \cdots . \tag{A6}$$

Thus, it is obvious that the diagonal elastic constants C_{kk} ($k=4$, 5, or 6) are given by

$$C_{kk} = C_{kk}^0 + 2m_k\rho^2 . \tag{A7}$$

To derive the other constants,

$$C_{ij} = \frac{\partial\sigma_i}{\partial e_j} \quad (i,j=1, 2, \text{ or } 3) , \tag{A8}$$

we notice that the resolution of the system (A2)–(A6) in the presence of longitudinal elastic stresses σ_i is formally identical to that of the free crystal. Actually, the elimination of e_j with the help of (A2),

$$e_j = \sum_{i=1}^{3} s_{ij}^0 (\sigma_i - m_i\rho^2) ,$$

shows that ρ and ϕ still verify the same equations as in the free-crystal case, if we replace α in these equations by

$$\alpha(\sigma_i) = \alpha + 2 \sum_{p,q=1}^{3} s_{pq}^0 m_p \sigma_q . \tag{A9}$$

Therefore, relation (A8) between the longitudinal strains and their conjugated stresses becomes

$$e_j = \sum_{i=1}^{3} s_{ij}^0 \left[\sigma_i - m_i\rho_s^2 \left[T + \frac{2}{a} \sum_{p,q=1}^{3} s_{pq}^0 m_p \sigma_q \right] \right] . \tag{A10}$$

The differentiation of this equation gives the elasticity tensor components

$$s_{ij} = s_{ij}^0 - \frac{2}{a} \frac{d\rho^2}{dT} \sum_{k,k'=1} s_{ik}^0 s_{k'j}^0 m_k m_{k'} , \tag{A11}$$

and, by inversion, the elastic constants

$$C_{ij} = C_{ij}^0 - \frac{2m_i m_j}{2 \sum_{k,k'=1}^{3} s_{kk'}^0 m_k m_{k'} - \frac{a}{d\rho_s^2/dT}} . \tag{A12}$$

[1]J. Petzelt, Phase Transitions **2**, 155 (1981).

[2]M. V. Klein, in *Light Scattering Near Phase Transitions*, edited by V. M. Agranovitch and A. A. Maradudin (North-Holland, Amsterdam, 1983).

[3]J. Schneck, J. C. Toledano, C. Joffrin, J. Aubree, B. Joukoff, and A. Gabelotaud, Phys. Rev. B **25**, 1766 (1982).

[4]J. Schneck and F. Denoyer, Phys. Rev. B **23**, 383 (1981).

[5]V. Dvorak, V. Janovec, and Y. Ishibashi, J. Phys. Soc. Jpn. **52**, 2053 (1983).

[6]G. Errandonea, J. C. Toledano, A. Litzler, H. Savary, J. Schneck, and J. Aubree, J. Phys. Lett. **45**, L329 (1984).

[7]J. Schneck, G. Calvarin, and J. M. Kyat, Phys. Rev. B **29**, 1476 (1984).

[8]J. P. Jamet and P. Lederer, J. Phys. Lett. **44**, L257 (1983).

[9]P. Lederer, G. Montambaux, J. P. Jamet, and M. Chauvin, J. Phys. Lett. **45**, L627 (1984).

[10]M. Mashiyama, S. Tanizahi, and K. Hamano, J. Phys. Soc. Jpn. **51**, 2538 (1982).

[11]H. G. Unruh, J. Phys. C **16**, 3245 (1983).

[12]P. B. Jamieson, S. C. Abrahams, and J. L. Bernstein, J. Chem. Phys. **50**, 4352 (1969).

[13]S. Singh, D. A. Draegertand, and J. E. Geusiu, Phys. Rev. B **2**, 2709 (1970).

[14]J. Schneck, J. Primot, J. Ravez, and R. Von der Muhl, Solid State Commun. **21**, 57 (1977).

[15]E. A. Giess, B. A. Scott, G. Burns, D. F. O'Kane, and A. Segmüller, J. Am. Ceram. Soc. **52**, 276 (1969).

[16]J. C. Toledano, J. Schneck, and G. Errandonea, in *Incommensurate Phases in Dielectrics*, edited by R. Blinc and A. P. Levanuyk (North-Holland, Amsterdam, 1985).

[17]J. C. Toledano, M. Busch, and J. Schneck, Ferroelectrics **26**, 775 (1976).

[18]J. C. Toledano and M. Busch, J. Phys. Lett. **36**, L141 (1975).

[19]J. C. Toledano, Phys. Rev. B **12**, 943 (1975); M. Busch, thèse de troiseme cycle, Université Paris VI (1974).

[20]T. Yamada, H. Iwasaki, and N. Niizeki, J. Appl. Phys. **41**, 4141 (1970).

[21]P. W. Young and J. F. Scott, Ferroelectrics **52**, 35 (1983); P.

W. Young, J. F. Scott, and B. B. Lavrencic, *ibid.* **53**, 327 (1984).

[22]G. Errandonea (unpublished).

[23]J. G. Dil, Rep. Prog. Phys. **45**, 285 (1982).

[24]R. Vacher and L. Boyer, Phys. Rev. B **6**, 639 (1970).

[25]D. Landau and E. Lifshitz, *Electrodynamique des milieux continus* (Mir, Moscow, 1969).

[26]J. S. Abell, K. G. Barradough, I. R. Harris, A. W. Verer, and B. Cockayne, J. Mater. Sci. **6**, 1084 (1971).

[27]A. W. Warner, G. A. Coquin, and J. L. Fink, J. Appl. Phys. **40**, 4353 (1969).

[28]J. F. Nye, *Physical Properties of Crystals* (Oxford University Press, New York, 1972).

[29]C. Kittel, *Introduction à la physique de l'état solide* (Bordas, Paris, 1972).

[30]A. Boudou and J. Sapriel, Phys. Rev. B **21**, 61 (1980).

[31]A. P. Levanyuk and D. G. Sannikov, Fiz. Tverd Tela (Leningrad) **18**, 423 (1976) [Sov. Phys.—Solid State **18**, 245 (1976)].

[32]V. Dvorák, and Y. Ishibashi, J. Phys. Soc. Jpn. **45**, 775 (1978).

[33]A. D. Bruce, R. A. Cowley, and A. F. Murray, J. Phys. C **11**, 3591 (1978).

[34]J. C. Toledano, J. Schneck, and C. Lamborelle, in *Symmetries and Broken Symmetries,* edited by N. Boccara (IDSET, Paris, 1981).

[35]C. J. de Pater, V. D. Axe, and R. Currat, Phys. Rev. B **19**, 4684 (1979).

[36]Y. Dvorák, Ferroelectrics **7**, 1 (1974).

[37]P. Bak and V. Emery, Phys. Rev. Lett. **36**, 978 (1976).

[38]Y. Ishibashi and H. Shiba, J. Phys. Soc. Jpn. **45**, 409 (1978).

[39]D. Durand, F. Denoyer, D. Lefur, R. Currat, and L. Bernard, J. Phys. (Paris) Lett. **44**, L207 (1983).

[40]P. Lederer and C. M. Chaves, J. Phys. (Paris) Lett. **42**, L127 (1981).

[41]A. P. Levanyuk, V. V. Osipov, A. S. Sigov, and A. A. Sobyanin, Zh. Eksp. Teor. Fiz. **76**, 345 (1979) [Sov. Phys.—JETP **49**, 176 (1979)].

[42]A. P. Levanyuk, Zh. Eksp. Teor. Fiz. **49**, 1304 (1965) [Sov. Phys.—JETP **22**, 901 (1966)].

[43]W. Yao, H. Z. Cummins, and R. H. Bruce, Phys. Rev. B **24**, 426 (1981).

[44]P. A. Fleury and K. Lyons, in *Structural Phase Transitions I,* edited by K. A. Muller and H. Thomas (Springer, Berlin, 1981).

[45]G. Errandonea, H. Savary, and J. Schneck, Ferroelectrics **55**, 19 (1984).

[46]J. M. Courdille and J. Dumas, J. Phys. (Paris) Lett. **36**, L5 (1975).

[47]T. Yagi, Y. Hidaka, and K. Miura, J. Phys. Soc. Jpn. **51**, 3562 (1982); I. Hatta, M. Hanami, and K. Hamano, *ibid.* **48**, 160 (1979).

[48]G. Hauret and J. P. Benoit, Ferroelectrics **40**, 1 (1982); W. Rewald and A. Vonlanthen, Solid State Commun. **38**, 209 (1981); Y. Luspin, M. Chabin, G. Hauret, and F. Gilleta, J. Phys. C **15**, 1581 (1982).

[49]W. Rehwald, and A. Vonlanthen, J. Phys. C **15**, 5361 (1982); J. P. Benoit, F. Thomas, and J. Berger, J. Phys. (Paris) **44**, 841 (1983).

[50]B. Berge, G. Dolino, and M. Vallade, J. Phys. (Paris) **45**, 715 (1984).

[51]L. D. Landau and I. M. Khalatnikov, Dokl. Akad. Nauk (SSSR) **96**, 469 (1954).

[52]H. Poulet and R. M. Pick, J. Phys. C **14**, 2675 (1981).